International Journal of Modern Physics B
2150204 (19 pages)

DOI: 10.1142/S0217979221502040

A comparative study of MHD fluid-particle suspension induced by metachronal wave under the effects of lubricated walls

Mubbashar Nazeer*, Farooq Hussain†, Laiba Shabbir‡, Adila Saleem‡, M. Ijaz Khan§,¶, M. Y. Malik‖, Tian-Chuan Sun**,†† and A. Hussain†

*Department of Mathematics, Institute of Arts and Sciences, Government College University Faisalabad Chiniot Campus, 35400, Pakistan

†Department of Mathematical Sciences (FBAS) BUITEMS, Quetta 87300, Pakistan

‡Department of Mathematics, Riphah International University Faisalabad Campus, 38000, Pakistan

§Department of Mathematics and Statistics, Riphah International University I-14, Islamabad 44000, Pakistan

¶Nonlinear Analysis and Applied Mathematics (NAAM) Research Group, Department of Mathematics, Faculty of Science, King Abdulaziz University, P. O. Box 80257, Jeddah 21589, Saudi Arabia

‖Department of Mathematics, College of Sciences, King Khalid University, Abha 61413, Kingdom of Saudi Arabia

**Qiuzhen College, Huzhou University, Huzhou 313000, P. R. China

††suntch@zjhu.edu.cn

Received 13 April 2021
Revised 6 June 2021
Accepted 8 June 2021
Published 31 July 2021

In this paper, the two-phase flow of non-Newtonian fluid is investigated. The main source of the flow is metachronal waves which are caused by the back and forth motion of cilia attached to the opposite walls of the channel. Magnetohydrodynamics (MHD) of Casson fluid experience the effects of transverse magnetic fields incorporated with the slippery walls of the channel. Thermal effects are examined by taking Roseland's approximation and application of thermal radiation into account. The heat transfer through the multi-phase flow of non-Newtonian fluid is further, compared with Newtonian bi-phase flow. Since the main objective of the current study is to analyze heat transfer through an MHD multiphase flow of Casson fluid. The two-phase heated flow of non-Newtonian fluid is driven by cilia motion results in nonlinear and coupled differential equations which are transformed and subsequently, integrated subject to slip boundary conditions. A closed-form solution is eventually obtained form that effectively describes the flow dynamics of multiphase flow. A comprehensive parametric study is carried out which highlights the significant contribution of pertinent parameters of the heat transfer of Casson multiphase flow. It is inferred that lubricated walls and magnetic fields hamper the movement of

††Corresponding author.

multiphase flow. It is noted that a sufficient amount of additional thermal energy moves into the system, due to the Eckert number and Prandtl number. While thermal radiation acts differently by expunging the heat transfer. Moreover, Casson multiphase flow is a more suitable source of heat transfer than Newtonian multiphase flow.

Keywords: Casson fluid; methachronal wave; slip conditions; heat transfer; magnetic field.

PACS numbers: 47.10.A−, 47.11.−j, 47.45.Gx, 44.35.+c, 44.40.+a

Nomenclature

$\bar{U}_{f,p}$:	Horizontal velocity of fluid	$\bar{V}_{f,p}$:	Vertical velocity of fluid
$\bar{X}, \bar{Y}$:	Horizontal and vertical coordinates	λ:	Wavelength
$\bar{t}$:	Time	$\bar{a}$:	Mean radius of channel
$\bar{c}$:	Wave velocity	ρ:	Fluid's density
k:	Thermal conductivity	$\bar{C}$:	Fractional density
c:	Specific heat	B_0:	Magnetic field
σ:	Electrical conductivity	μ_s:	Fluid's viscosity
ω_v:	The relaxation time of velocity	ω_T:	The relaxation time of temperature
Q_r:	Radiative heat flux	μ_0:	Plastic viscosity
u_f:	Dimensionless fluid velocity	$\theta_{f,p}$:	Dimensionless fluid temperature
e:	Eccentricity parameter	P_v:	Particle volume fraction parameter
ζ:	Casson fluid parameter	Λ:	Slip parameter
γ:	Thermal slip parameter	e_k:	Eckert number
P_d:	Prandtl number	r_d:	Radiation parameter

1. Introduction

Cilia is a hair-like motile structure that forms on the surface of the diversity of eukaryotic cells. The back and forth beating of cilia results in metachronal waves. It is also a well-known fact that the successive motion of cilia, worm segments/legs, produce a wavy motion. Therefore, it is termed as "*Methachronal wave*". It is found in nature in abundance, from single-cell organisms, crustaceans, and insects. Bhatti *et al.*[1] provide heat transfer in fluid-particle suspension due to metachronal waves. The MHD flows are investigated under the impact of thermal radiation and with the help of approximated value of Roseland's law. In successive study pertains to magnetohydrodynamics of cilia-driven fluid-particle suspension through a porous channel, Akbar *et al.*[2,3] used the effects of magnetic field on the Casson fluid flows to investigate the metachronal beating of cilia, respectively by applying uniform and oblique magnetic fields. The study includes that there is a tremendous hip in the momentum of the fluid. A three-dimensional flow, generated by metachronal waves has been simulated by Quek *et al.*[4] The flow dynamics display that fluid

velocity hampered, due to surface tension caused by the top and bottom layers of fluid. Nazeer *et al.*[5] have elaborated in detail the removal of mucus from lungs and bloodstreams, as they mathematically modeled a bio-magnetic fluid bounded by ciliated walls of wavy channel incorporated with viscous dissipation. Some notable papers on the metachronal motion can be seen in Refs. 6–8.

Magnetohydrodynamics (MHD) is a well-known phenomenon of fluids, related to the study of electrically conducting fluids. The implementation of Magnetohydrodynamics is very wide in biomedical sciences, engineering, astrophysics, geophysics, sensor, and magnetic drug targeting.[9–17] Mebarak-Oudina *et al.*[18] numerically analyzed the stability of natural convection through a cylindrical annulus in presence of radial magnetism and presented various important results for involved parameters. Zaim *et al.*[19,20] established a mathematical model to investigate an MHD natural convection flow of nanofluid (Cu-Water) with the help of the Galerkin Element Method. The numerical expressions for velocity, Nusselt number, streamlines, and isotherms were presented by them. The analysis of convective heat transfer and discrete heat source for titanic nanofluids through cylindrical annulus presented by Mebarek-Oudina.[21]

Lubrication effects are effectively used to expunge skin friction caused by the rough surfaces, mainly in industries and medical sciences. Ramesh *et al.*[22] studied the effects of slippery walls on an MHD flow of Jeffrey fluid through the microchannel. Unlike, the previously mentioned studies Nazeer *et al.*[23] applied the velocity slip condition and, as well as, thermal slip boundary conditions on the magnetohydrodynamics of multiphase flow. Similar types of flows under the impact of lubrication effects are discussed in the following studies.[24–26]

Heat transfer is the most important mechanical phenomenon. It occurs due to temperature differences. In this process, thermal energy moves from a region of higher temperature to a region of lower temperature via three fundamental modes of heat transfer namely; convection, conduction, and radiation. Fei *et al.*[27] studied the impact of rotation speed and characteristics of heat transfer on fluid flow. The rotation of the spiral tube is used to improve the heat transfer rate. Rohachev *et al.*[28] presented the analysis on the regulation of surface with different sort of finning under forced air convection. In a combined air-cooling system, the developed heat transfer surface can be used. Wang *et al.*[29] addressed the representative experimental data for the available heat transfer model and drop-wise condensation on a smooth hyperbolic surface. Due to the thickness of the promoter layer, the condensation heat transfer reduces and decreases the nucleation density. Some interesting studies on multiphase flows are mentioned in Refs. 30–34.

It is evident from the literature survey that no attention has been made, toward the comparative analysis of heat transfer through Casson multiphase flow and Newtonian multiphase flow which are driven by the motile motion of cilia structure. Since most of the mechanical, industrial, and physiological flows are highly viscous and multi-components. Therefore, a fruitful effort is made in this connection to address the missing theoretical problem.

2. Mathematical Modeling

Consider an unsteady two-dimensional and electrically conducting Casson fluid through a channel as shown in Fig. 1. The hydro-magnetic multiphase flow is due to the metachronal waves which travel along the opposite walls. Methachronal waves[1] produced by the sequential beating of tiny hair-like structures are given as

$$\bar{Y} = \bar{F}(\bar{X}, \bar{t}) = \bar{a} + \bar{a} \in \mathrm{Cos}\frac{2\pi}{\lambda}(\bar{X} - \bar{c}\bar{t}), \tag{1}$$

$$\bar{X} = \bar{G}(\bar{X}, \bar{t}) = \bar{X}_0 + \bar{a} \in \alpha\,\mathrm{Cos}\frac{2\pi}{\lambda}(\bar{X} - \bar{c}\bar{t}), \tag{2}$$

where $\bar{X}$ and $\bar{Y}$represent coordinates, $\bar{c}$ is the velocity of the wave, λ is the wavelength, $\bar{t}$ is time, and $\bar{a}$ is the mean radius of the channel. Therefore, the transport of cilia structure along horizontal and vertical directions is defined as[1,35]

$$\bar{U}_{f,p} = \frac{\frac{-2\pi}{\lambda}\bar{a} \in \alpha\bar{c}\,\mathrm{Cos}\frac{2\pi}{\lambda}(\bar{X} - \bar{c}\bar{t})}{1 - \frac{-2\pi}{\lambda}\bar{a} \in \alpha\mathrm{Cos}\frac{2\pi}{\lambda}(\bar{X} - \bar{c}\bar{t})}, \tag{3}$$

$$\bar{V}_{f,p} = \frac{\frac{-2\pi}{\lambda}\bar{a} \in \alpha\bar{c}\,\mathrm{Sin}\frac{2\pi}{\lambda}(\bar{X} - \bar{c}\bar{t})}{1 - \frac{-2\pi}{\lambda}\bar{a} \in \alpha\mathrm{Sin}\frac{2\pi}{\lambda}(\bar{X} - \bar{c}\bar{t})}, \tag{4}$$

where 'f' and 'p' denote fluid and particulate phases, respectively. The flow equations for both phases are written as:

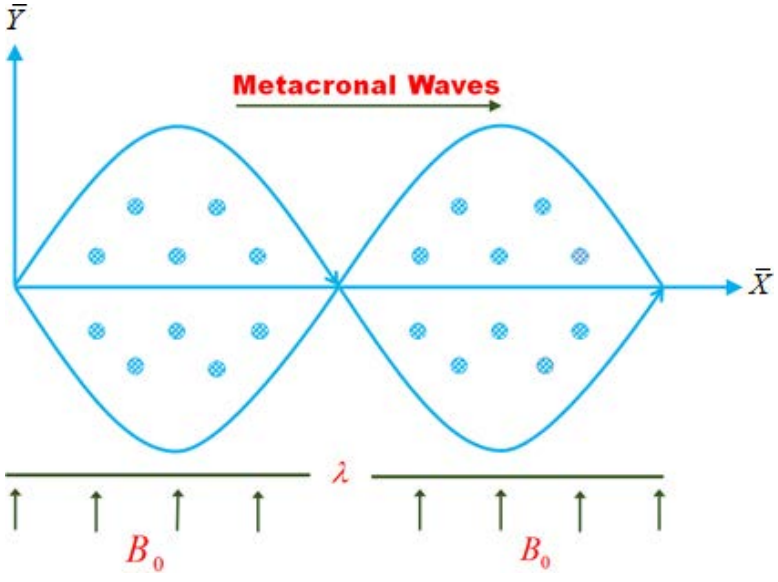

Fig. 1. (Color online) Geometry of flow problem.

2.1. *Fluid phase equations*

Since we are dealing with a two-dimensional flow of Casson fluid, the set of partial differential equations which are required to describe the conservation of mass and momentum of base liquid are[1,35]

$$\frac{\partial \bar{U}_f}{\partial \bar{X}} + \frac{\partial \bar{V}_f}{\partial \bar{Y}} = 0, \tag{5}$$

$$(1-\bar{C})\rho_f \left(\frac{\partial \bar{U}_f}{\partial \bar{t}} + \bar{U}_f \frac{\partial \bar{U}_f}{\partial \bar{X}} + \bar{V}_f \frac{\partial \bar{U}_f}{\partial \bar{Y}} \right) = -(1-\bar{C}) \frac{\partial \bar{P}}{\partial \bar{X}} + (1-\bar{C}) \left(\frac{\partial}{\partial \bar{X}} r_{\bar{X}\bar{X}} + \frac{\partial}{\partial \bar{Y}} r_{\bar{X}\bar{Y}} \right) + \frac{\bar{C}S}{\omega_v} (\bar{U}_p - \bar{U}_f) - \sigma B_0^2 \bar{U}_f, \tag{6}$$

$$(1-\bar{C})\rho_f \left(\frac{\overline{\partial V}_f}{\partial \bar{t}} + \bar{U}_f \frac{\partial \bar{V}_f}{\partial \bar{X}} + \bar{V}_f \frac{\partial \bar{V}_f}{\partial \bar{Y}} \right) = -(1-\bar{C}) \frac{\partial \bar{P}}{\partial \bar{Y}} + (1-\bar{C}) \left(\frac{\partial}{\partial \bar{X}} r_{\bar{X}\bar{X}} + \frac{\partial}{\partial \bar{Y}} r_{\bar{X}\bar{Y}} \right) + \frac{\bar{C}S}{\omega_v} (\bar{V}_p - \bar{V}_f). \tag{7}$$

2.2. *Particle phase equations*

Conservation of mass and momentum of particle phase are given as[1,35]

$$\frac{\partial \bar{U}_p}{\partial \bar{X}} + \frac{\partial \bar{V}_p}{\partial \bar{Y}} = 0, \tag{8}$$

$$\bar{C}\rho_p \left(\frac{\partial \bar{U}_p}{\partial \bar{t}} + \bar{U}_p \frac{\partial \bar{U}_p}{\partial \bar{X}} + \bar{V}_p \frac{\partial \bar{U}_p}{\partial \bar{Y}} \right) = -\bar{C} \frac{\partial \bar{P}}{\partial \bar{X}} + \frac{S\bar{C}}{\omega_v} (\bar{U}_f - \bar{U}_p), \tag{9}$$

$$\bar{C}\rho_p \left(\frac{\partial \bar{V}_p}{\partial \bar{t}} + \bar{U}_p \frac{\partial \bar{V}_p}{\partial \bar{X}} + \bar{V}_p \frac{\partial \bar{V}_p}{\partial \bar{Y}} \right) = -\bar{C} \frac{\partial \bar{P}}{\partial \bar{Y}} + + \frac{\bar{C}S}{\omega_v} (\bar{V}_f - \bar{V}_p), \tag{10}$$

where ω_T and ω_v denoted relaxation time of temperature and velocity. The drag force coefficient is defined as

$$S = \frac{9\mu_0}{2\underline{a}^2} \bar{\lambda}(\bar{C}). \tag{11}$$

In the above μ_0 denotes the viscosity of Casson fluid which is significant to determine the viscosity of the fluid-particle suspension

$$\mu_s = \frac{\mu_0}{1-\chi\bar{C}}. \tag{12}$$

In (13) and (14), one can identify

$$\bar{\lambda}(\bar{C}) = \frac{4}{(2-3\bar{C})} + \frac{3\sqrt{8\bar{C} - 3\bar{C}^2 + 3\bar{C}}}{(2-3\bar{C})}, \tag{13}$$

$$\chi = \frac{7}{100} e^{\left(\frac{249}{100}\bar{C} + \frac{1107}{T} e^{-\frac{169}{100}\bar{C}}\right)}. \tag{14}$$

2.3. *Heat transport equation*

$$(1-\bar{C})c_f * \rho_f \left(\frac{\partial \bar{T}_f}{\partial \bar{t}} + \bar{U}_f \frac{\partial \bar{T}_f}{\partial \bar{X}} + \bar{V}_f \frac{\partial \bar{T}_f}{\partial \bar{Y}}\right) = k\left(1-\bar{C}\right)\frac{\partial^2 \bar{T}_f}{\partial \bar{Y}^2} + \frac{ro_f \times c_f \bar{C}}{\omega_T}(\bar{T}_p - \bar{T}_f)$$
$$+ \frac{\bar{C}S}{\omega_v}(\bar{U}_f - \bar{U}_p)^2 + \mu_s(1-\bar{C})r_{\bar{X}\bar{Y}}\left(\frac{\partial \bar{U}_f}{\partial \bar{Y}}\right) - \frac{\partial Q_R}{\partial \bar{Y}}, \tag{15}$$

$$c_p \rho_f \bar{C}\left(\frac{\partial \bar{T}_p}{\partial \bar{t}} + \bar{U}_p \frac{\partial \bar{T}_p}{\partial \bar{X}} + \bar{V}_p \frac{\partial \bar{T}_p}{\partial \bar{Y}}\right) = \frac{\rho_p \bar{C} c_p}{\omega_T}(\bar{T}_f - \bar{T}_p). \tag{16}$$

By Roseland's approximation, the expression of radiative heat flux is defined as

$$Q_r = -\frac{16\bar{\sigma}\bar{T}^3}{3\bar{k}}\frac{\partial \bar{T}}{\partial \bar{Y}}. \tag{17}$$

By defining the stress tensor for Casson fluid[36]

$$r_{ij} = \begin{cases} 2\varepsilon_{ij}\left(\mu_0 + \dfrac{\wp_y}{\sqrt{2\prod_c}}\right), & \prod_c < \prod, \\ 2\varepsilon_{ij}\left(\mu_0 + \dfrac{\wp_y}{\sqrt{2\prod_c}}\right), & \prod_c > \prod, \end{cases} \tag{18}$$

where ε_{ij} is deformation rate component, $\prod$ is a product of deformation rate, Π_c is the critical value of product-based and μ_0 is plastic viscosity. Using the following given transformation to convert fixed frame to wave frame, we have

$$\begin{aligned} &\bar{x} = \bar{X} - \bar{c}\bar{t}, \quad \bar{y} = \bar{Y}, \quad \bar{u}_f = \bar{U}_f - \bar{c}, \\ &\bar{v}_f = \bar{V}_f, \quad \bar{u}_p = \bar{U}_p - \bar{c}, \quad \bar{v}_p = \bar{V}_p, \quad \bar{p} = \bar{P}. \end{aligned} \tag{19}$$

And, subsequently, applying nondimensional variables and parameters in the governing equations, we have

$$\left.\begin{aligned} &x = \frac{\bar{x}}{\lambda}, \quad y = \frac{\bar{y}}{\bar{a}}, \quad u_{f,p} = \frac{\bar{u}_{f,p}}{\bar{c}}, \quad P_r = \frac{\mu_s c}{k}, \quad v_{f,p} = \frac{\bar{v}_{f,p}}{\bar{c}\delta}, \\ &p = \frac{\bar{a}^2}{\lambda \mu_s \bar{c}}\bar{p}, \quad \mathrm{Re} = \frac{\rho \bar{a}\bar{c}}{\mu_s}, \quad N = \frac{S\bar{a}^2}{\mu_s \omega_v}, \quad H = \sqrt{\frac{B_0^2 \sigma \bar{a}^2}{\mu_s}}, \\ &\theta_{f,p} = \frac{\bar{T}_{f,p} - \bar{T}_0}{\bar{T}_1 - \bar{T}_0}, \quad e_k = \frac{\bar{c}^2}{c(\bar{T}_1 - \bar{T}_0)}, \quad r_d = \frac{4\bar{T}^3\bar{\sigma}}{\mu_s c \bar{k}}, \quad \Phi = \frac{\bar{b}}{\bar{a}}. \end{aligned}\right\} \tag{20}$$

Considering the long-wavelength assumption and low Reynolds approximation finally, the governing equations after some necessary manipulation transform into the following:

$$\left(1 + \frac{1}{\zeta}\right)\frac{\partial^2 u_f}{\partial y^2} - H^2(u_f + 1) - \left(\frac{1}{1-\bar{C}}\right)\frac{dp}{dx} = 0, \tag{21}$$

$$\left(\frac{1}{P_d} + \frac{4}{3}r_d\right)\frac{\partial^2 \theta_f}{\partial y^2} + e_k\left(1 + \frac{1}{\zeta}\right)\left(\frac{\partial u_f}{\partial y}\right)^2 + \frac{e_k}{N(1-\bar{C})}\left(\frac{dp}{dx}\right)^2 = 0. \tag{22}$$

The expression for pressure gradient and temperature of both phases can be obtained as

$$\frac{1}{N}\frac{dp}{dx} = (u_f - u_p), \tag{23}$$

$$\theta_f = \theta_p. \tag{24}$$

2.4. *Boundary conditions*

In order to minimize the wall friction, the lubrication effects are applied on the opposite walls of the channel. Therefore, the momentum and thermal boundary conditions are chosen as:

$$\text{(i)} \qquad \frac{\partial}{\partial y}u_f(0) = 0, \quad u_f(h) + 1 = -\frac{2\pi\Phi\alpha\beta\cos 2\pi(x)}{1 - 2\pi\Phi\alpha\beta\cos 2\pi(x)} + \frac{\Lambda}{\zeta}\frac{\partial u_f(h)}{\partial y}, \tag{25}$$

$$\text{(ii)} \qquad \frac{\partial}{\partial y}\theta_f(0) = 0, \quad \theta_f(h) + \gamma\frac{\partial}{\partial y}\theta_f(h) = 1. \tag{26}$$

It is to be noted that e denotes the eccentricity of the elliptic path.

3. Solution of the Problem

Equations (21)–(22) are coupled and nonlinear differential equations which are integrated subject to the boundary conditions (25)–(26) which yield the transport of Casson fluid and particles given as

$$u_f = \frac{(1 + a + BP)(2\,\mathrm{Cosh}[Ay]) - 1 - BP)}{2(\zeta\,\mathrm{Cos}[Ah] - A\Lambda\,\mathrm{Sinh}[Ah])}, \tag{27}$$

$$u_p = \frac{(1 + a + BP)}{2(\zeta\,\mathrm{Cos}[Ah] - A\Lambda\,\mathrm{Sinh}[Ah])}\left(2\,\mathrm{Cosh}[Ay]) - 1 - BP - \frac{P}{N}\right). \tag{28}$$

Similarly, the expression for heat transport through the multiphase flow is

$$\theta = c_3 + a_1 y^2 + a_2\,\mathrm{Cosh}[2Ay]. \tag{29}$$

In the above equation, the constant is identified as

$$c_3 = \frac{\begin{array}{c}-8L_1 + 2A^2h^2L^2L_2 + 4A^2hL^2L_2\gamma - L^2L_2\,\mathrm{Cosh}[2Ah] \\ - 2AL^2L_2\gamma\,\mathrm{Sinh}[2Ah] - 4h^2L_3 - 8h\gamma L_3\end{array}}{8L_1}. \tag{30}$$

Now, to determine a separate expression for the volumetric flow rate of Casson fluid and particle with the help of the following equations, we have

$$Q_f = (1 - \bar{c})\left(\frac{(1 + a + BP)\zeta(2\,\mathrm{Sinh}[Ay])}{2(\zeta\,\mathrm{Cosh}[Ah] - A\Lambda\,\mathrm{Sinh}[Ah])} - h - BPh\right), \tag{31}$$

$$Q_p = \bar{c}\left(\frac{(1 + a + BP)\zeta(2\,\mathrm{Sinh}[Ay])}{2(\zeta\,\mathrm{Cosh}[Ah] - A\Lambda\,\mathrm{Sinh}[Ah])} - h - BPh - \frac{hP}{N}\right). \tag{32}$$

The total volume flow rate is

$$Q = Q_p + Q_f - 1, \tag{33}$$

$$Q = \begin{pmatrix} (1-\bar{C})\left(-h - BhP + \dfrac{(1+a+BP)\zeta \sinh[Ah]}{A(\zeta \cosh[Ah] - A\Lambda \sinh[Ah])}\right) + \bar{C} \\ \left(-h - BhP + \dfrac{(1+a+BP)\zeta \sinh[Ah]}{A(\zeta \cosh[Ah] - A\Lambda \sinh[Ah])} - \dfrac{hP}{N_1}\right) - 1, \end{pmatrix}. \tag{34}$$

The contribution of pressure gradient in the current heat transfer through multiphase flow is very significant. The pressure gradient is given by the following expression:

$$P = \frac{(A(h+Q)\zeta \,\mathrm{Cosh}[Ah] - (A^2(h+Q)\Lambda + (1+a)\zeta)\,\mathrm{Sinh}[Ah]N}{-Ah\,\mathrm{Cosh}[Ah](c+BN) + \mathrm{Sinh}[Ah](A^2 ch\Lambda + B(A^2 h\Lambda + \zeta)N)}. \tag{35}$$

4. Results and Discussion

This section is dedicated to the parametric study which graphically shows the altering behavior of heat and mass transfer of Casson fluid. The pertinent parameters which are taken into account to analyze their contribution include wavenumber (λ), a measure of the eccentricity parameter (e), particle volume fraction (P_v), Casson fluid parameter (ζ), slip parameter (Λ), Thermal slip parameter (γ), Eckert number (e_k), Prandtl number (P_r), and radiation parameter (r_d).

As the current investigation is a comparative analysis of Casson multiphase flow with Newtonian multiphase flow, subject to apply slip boundary conditions. Here, we also present the comparison between Newtonian and non-Newtonian fluid by sketching several graphs for various parameters. Graphs with dashed ($\zeta \to 1$) represent the Casson multiphase flow, while solid sketches ($\zeta \to \infty$) are used for Newtonian bi-phase flow. For convenience, this portion is further divided into subsections to elaborate findings in detail.

4.1. *Flow analysis*

In this section variation in the flow of base, the liquid is examined against the selected parameters in Figs. 2–5, respectively. Figure 2 depicts the velocity profile of each type of flow against different values of eccentricity parameter (e). It is noted that the momentum of the flow increases for both Newtonian fluid and Casson fluid in the region $y < 0.6$. But, there is an opposite trend in the momentum of the fluid. It is observed that in the region for $y > 0.6$, each velocity of the flow keeps on reducing rapidly. However, the shear thickening effects are so dominant in the non-Newtonian fluid which enhances the viscous forces. Therefore, the transport of Casson fluid is much slower than Newtonian fluid as shown in the diagram.

In Fig. 3, the variation of wavenumber is spotted. Wavenumber is defined as the number of waves per unit distance ($\lambda = \frac{1}{\lambda}$). It is very interesting to note that wave number and velocity are inversely related to each other. It is examined that

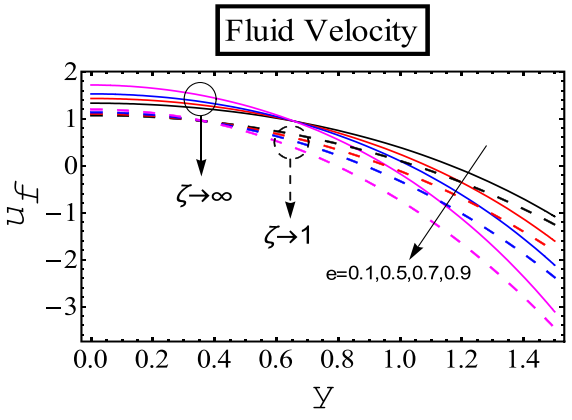

Fig. 2. (Color online) Velocity profile u_f for e when $\Lambda = 0.05$, $\lambda = 0.2$, $H = 1$, $e_k = 0.5$, $P_v = 0.2$, $r_d = 3$.

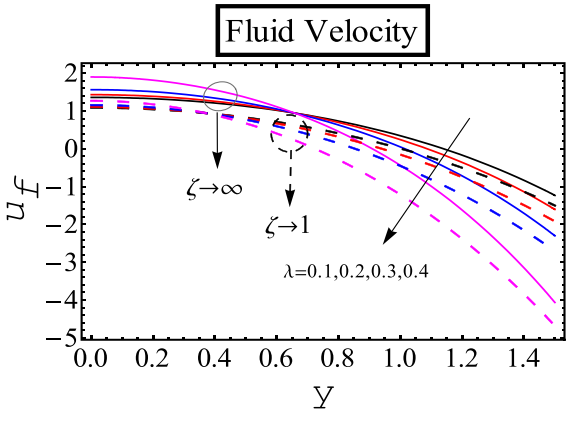

Fig. 3. (Color online) Velocity profile u_f for λ when $\Lambda = 0.05$, $e = 0.5$, $H = 1$, $e_k = 0.5$, $P_v = 0.2$, $r_d = 3$.

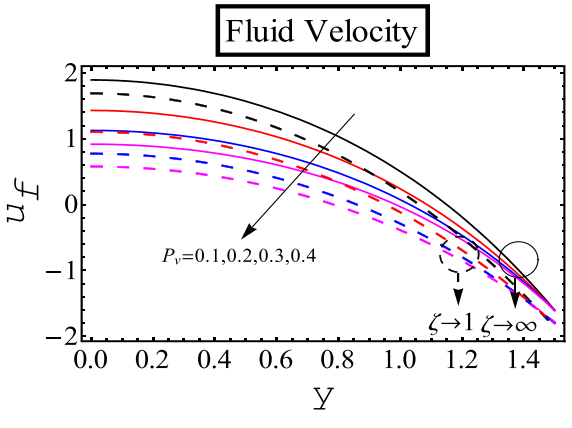

Fig. 4. (Color online) Velocity profile u_f for P_v when $\Lambda = 0.05$, $e = 0.5$, $H = 1$, $e_k = 0.5$, $\lambda = 0.2$, $r_d = 3$.

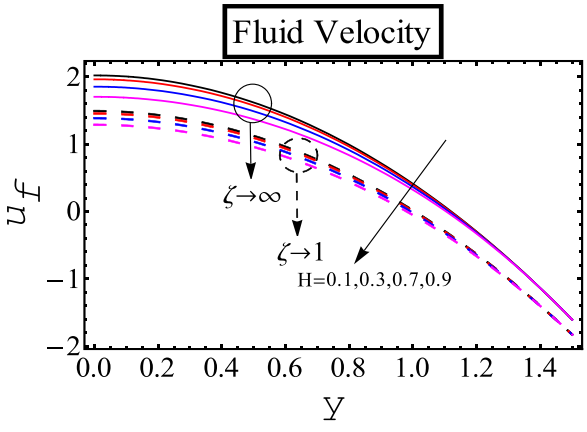

Fig. 5. (Color online) Velocity profile for H when $\Lambda = 0.05$, $e = 0.5$, $H = 1$, $e_k = 0.5$, $\lambda = 0.2$, $r_d = 3$.

by increasing the value of (λ) the velocity of base fluid increases in the region $y < 0.6$ while u_f decreases for $y > 0.6$. Figure 4 shows that there is an inverse relationship between velocity profile u_f and volume fraction P_v. We can see that increment the value P_v causes the velocity of the base fluid to reduce. Finally, the role of magnetic fields on the multiphase flow is investigated in Fig. 5. It is examined that by increasing the value of the Hartman number the velocity profile decreases. Hartman number produces Lorentz force, and Lorentz force is a force that opposes the flow and is produced when the magnetic field is applied to electrically conducting fluid. Due to the influence of Lorentz forces, magnetic fields oppose the flow.

4.2. *Thermal analysis*

This section is about the heat transferred by both phases from the region of higher temperature to a region of lower temperature. Figures 6–8 discuss the temperature profile ($\theta_{f,p}$) of Newtonian fluid and non-Newtonian fluid against different parameters. Figure 6 shows the contribution of the Prandtl number (P_r). It can be noticed that heat transfer rate enhances with respect to the dimensionless quantity because the Prandtl number (P_r) exhibits direct relation by enhancing the values of P_v. On the contrary, the heat transfer is much better in Casson fluid flow as compared to the Newtonian case. This can also be inferred from the fact that force of friction or resistance between adjacent fluid particles in Casson fluid, adds extra heat into the system due to its less momentum/velocity. In Fig. 7, a rise in temperature profile ($\theta_{f,p}$) against the increasing values of the Eckert number (e_k) is observed. This is because increasing values of Eckert number increased vibration of fluid due to large kinetic energy which results in collision of fluid particles. Hence, the rapid collision of molecules enhances the dissipation of heat in the boundary layer, which heightens the temperature field. Figure 8 shows an altogether different phenomenon in the temperature profile. Unlike, in the previous two cases, the heat

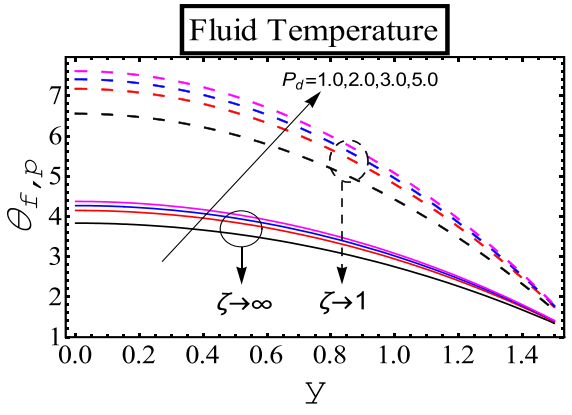

Fig. 6. (Color online) Temperature profile $\theta_{f,p}$ for P_d when $\Lambda = 0.05$, $\gamma = 0.1$, $e = 0.5$, $H = 1$, $e_k = 0.5$, $\lambda = 0.2$, $r_d = 3$.

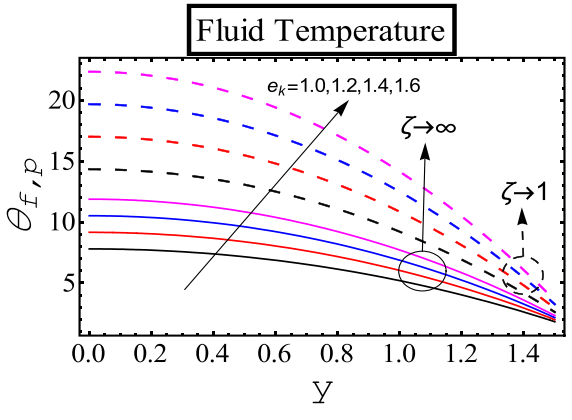

Fig. 7. (Color online) Temperature profile $\theta_{f,p}$, for e_k when $\Lambda = 0.05$, $\gamma = 0.1$, $e = 0.5$, $H = 1$, $r_d = 3.0$, $\lambda = 0.2$, $P_v = 0.2$.

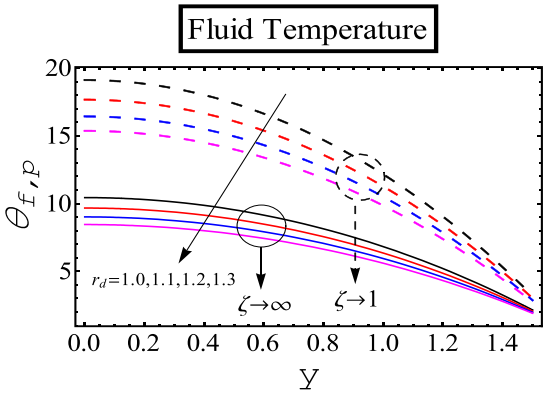

Fig. 8. (Color online) Temperature profile $\theta_{f,p}$, for r_d when $\Lambda = 0.05$, $\gamma = 0.1$, $e = 0.5$, $H = 1$, $e_k = 0.5$, $\lambda = 0.2$, $P_v = 0.2$.

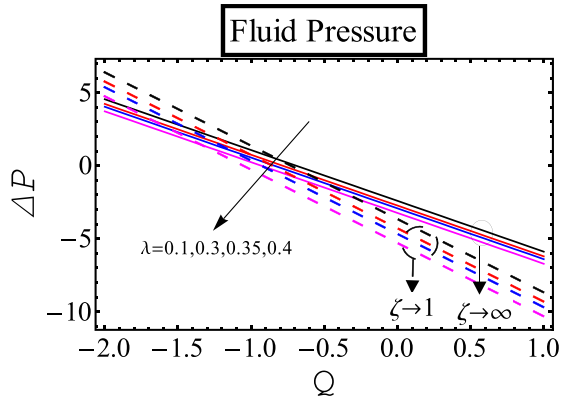

Fig. 9. (Color online) Pressure rise versus volume flow rate for λ when $\Lambda = 0.05$, $e = 0.5$, $H = 1$, $e_k = 0.5$, $\lambda = 0.2$, $P_v = 0.2$.

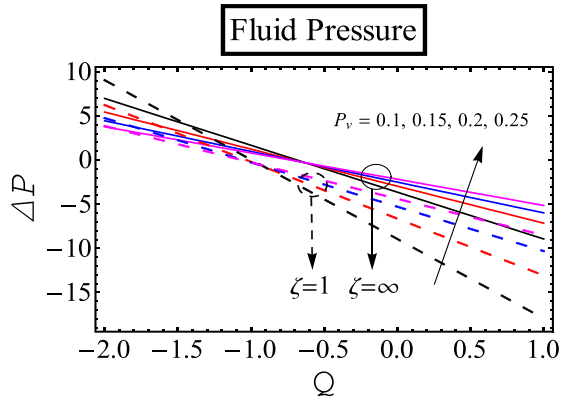

Fig. 10. (Color online) Pressure rise versus volume flow rate for P_v when $\Lambda = 0.05$, $e = 0.5$ $r_d = 3$, $e_k = 0.5$, $\lambda = 0.2$, $H = 1$.

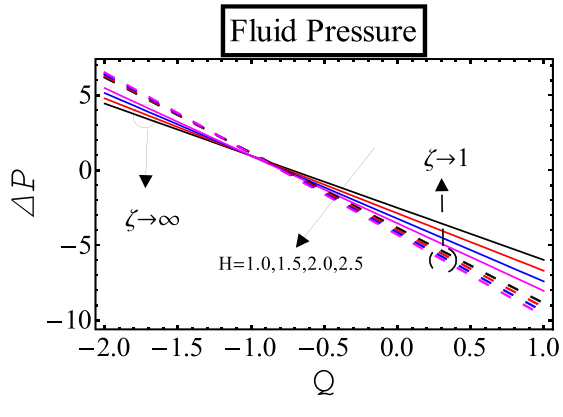

Fig. 11. (Color online) Pressure rise versus volume flow rate for H when $\Lambda = 0.05$, $e = 0.5$, $r_d = 3$, $e_k = 0.5$, $\lambda = 0.2$, $P_v = 0.2$.

transfer of multiphase flow reduces against increasing values of radiation parameter. Physically, when the radiation parameter increases to large values it yields the dominance effect of conduction over radiation. These results decrease in boundary layer thickness and increase in heat loss which decreases temperature profile.

4.3. *Influence of pressure rise*

Flow caused by metachronal wave contribution of pressure rise is very significant. Figures 9–11 describe the role of pressure rise on heat transfer of multiphase flow

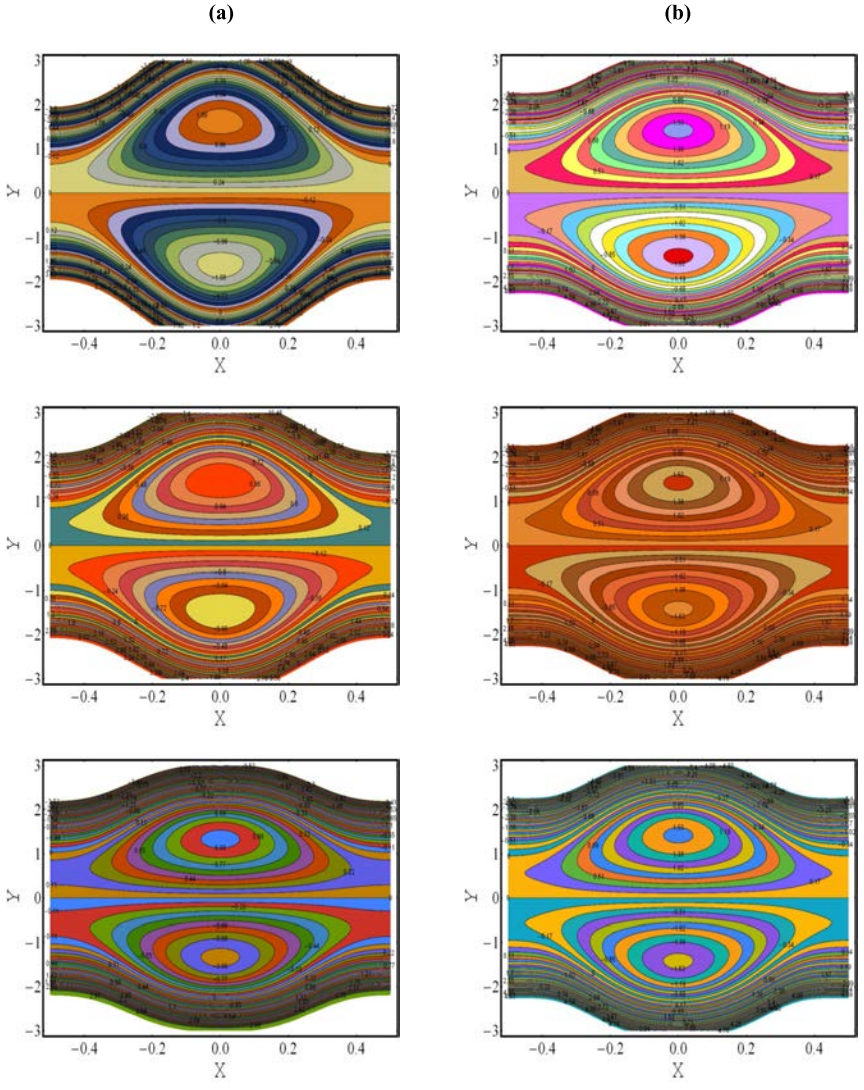

Fig. 12. (Color online) Streamlines for $e(0.1, 0.3, 0.5)$ when (a) $\Lambda = 0$, $\lambda = 0.2$, $P_v = 0.2$, $H = 1$, $\zeta = 1$. (b) $\Lambda = 0.2$, $\lambda = 0.2$, $P_v = 0.2$, $H = 1$, $\zeta = 1$.

against wave number (λ), particle volume fraction (P_v), and Hartmann number (H). The contribution of pressure rise acts differently depending on the four pumping regions namely; Retrograde pumping region ($\Delta P > 0, Q < 0$), peristaltic pumping region ($\Delta P > 0, Q > 0$), Free pumping region ($\Delta P < 0, Q < 0$), Co-pumping region ($\Delta P < 0, Q > 0$). Figure 9 displays the effects of wave number (λ) on pressure rise, it is observed that in all regions the wave number contributed equally. By increasing

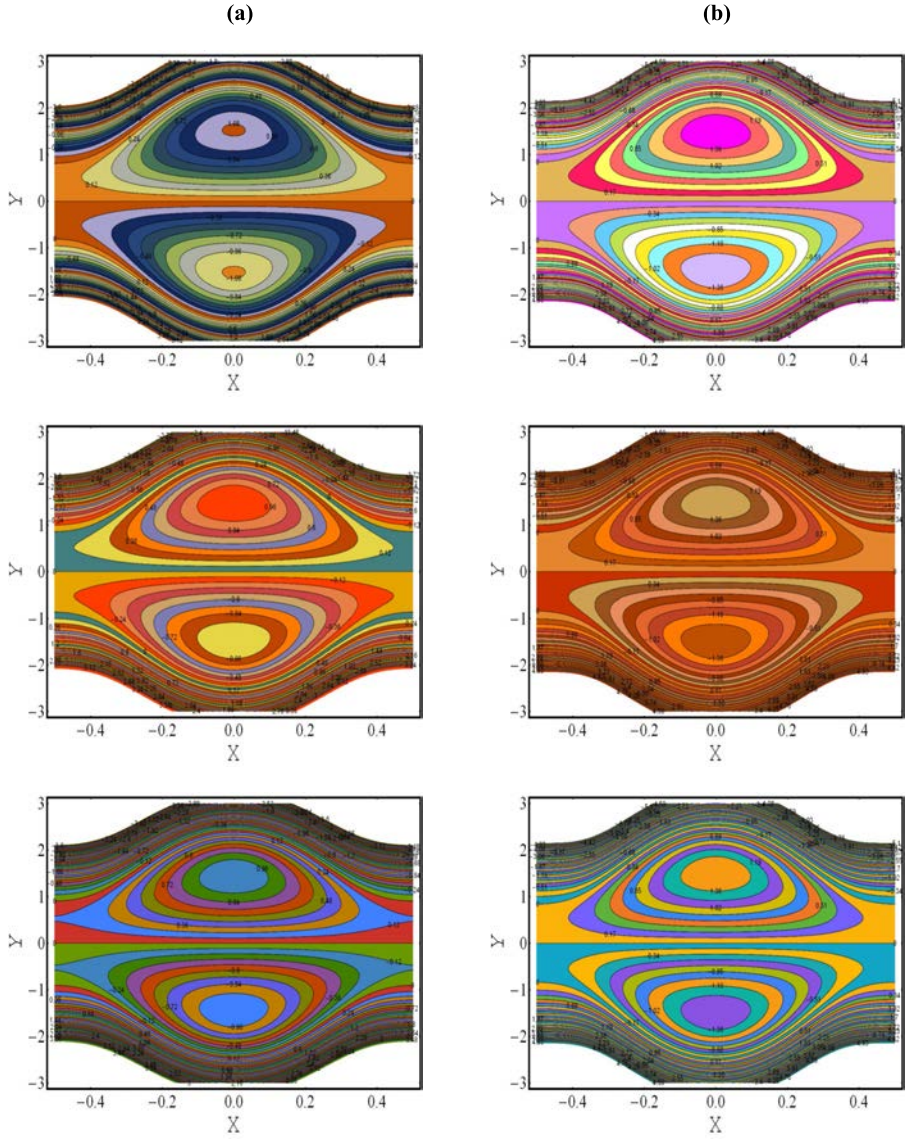

Fig. 13. (Color online) Streamlines for $\lambda(0.1, 0.12, 0.14)$ when (a) $\Lambda = 0$, $e = 0.5$, $P_v = 0.2$, $H = 1$, $\zeta = 1$. (b) $\Lambda = 0.2$, $e = 0.5$, $P_v = 0.2$, $H = 1$, $\zeta = 1$.

the quantity of wavenumber (λ), there is a vivid decline in the strength of pressure rise for both types of multiphase flows (i.e., $\zeta \to 1$ and $\zeta \to \infty$). In Fig. 10, the behavior of pressure against particle volume fraction (P_v) is plotted. It is interesting to note that in the retrograde pumping region volume fraction decreases while it has an opposite trend in the remaining regions. Variation in pressure rise due to Hartmann number (H) can be seen in Fig. 11. In the retrograde pumping region, Hartmann number (H) shows dual behavior for $Q < -1$, when Hartmann number

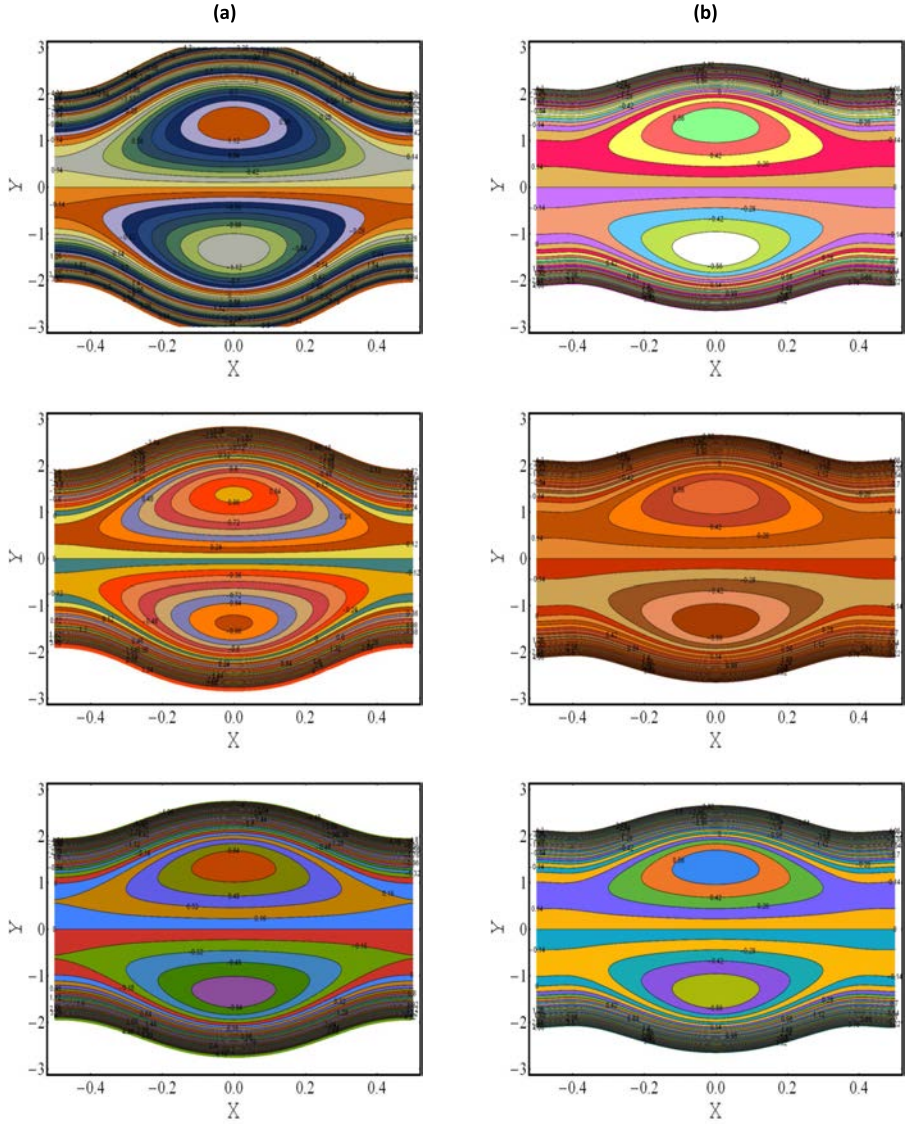

Fig. 14. (Color online) Streamlines for $H(1.0, 2.0, 3.0)$ when (a) $\lambda = 0.2$, $e = 0.5$, $\zeta = 1$, $P_v = 0.2$, $\Lambda = 0$. (b) $\lambda = 0.2$, $e = 0.5$, $\zeta = 1$, $P_v = 0.2$, $\Lambda = 0.2$.

(H) increases then a rise in pressure is observed. But pressure rise decreases when Hartmann number (H) increases when $Q > -1$ for both Newtonian and non-Newtonian fluid cases.

4.4. *Trapping phenomenon*

Back and forth motion of cilia structure introduces "*Trapping Phenomenon*". Emerging of circulating boluses is called the trapping phenomenon. Boluses are

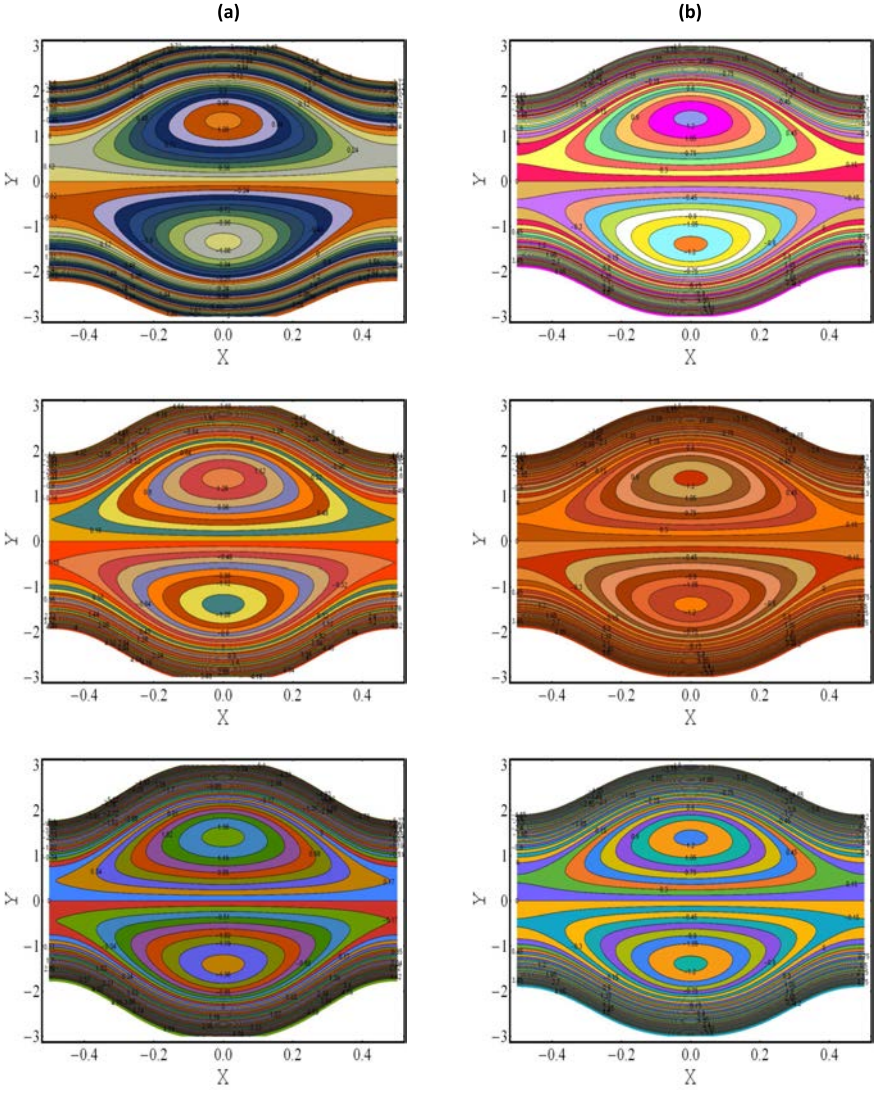

Fig. 15. (Color online) Streamlines for $\zeta(0.5, 2.0, \infty)$ when (a) $\lambda = 0.2$, $e = 0.5$, $H = 1$, $P_v = 0.2$, $\Lambda = 0$. (b) $\lambda = 0.2$, $e = 0.5$, $H = 1$, $P_v = 0.2$, $\Lambda = 0.2$.

caused by the wall resistance on the streamlines. Enclosed streamlines for both no-slip and slip boundary conditions have been graphed in Figs. 12–16 against eccentricity parameter, wavenumber, Casson fluid, Volume fraction, and Hartman number, respectively. In Fig. 12(a), we can observe that by increasing e the magnitude of bolus flattened passively while the number of boluses decreased and for both the cases e has no significant effect on the magnitude of bolus when slip condition applies on it as shown in Fig. 12(b), the magnitude is approximately

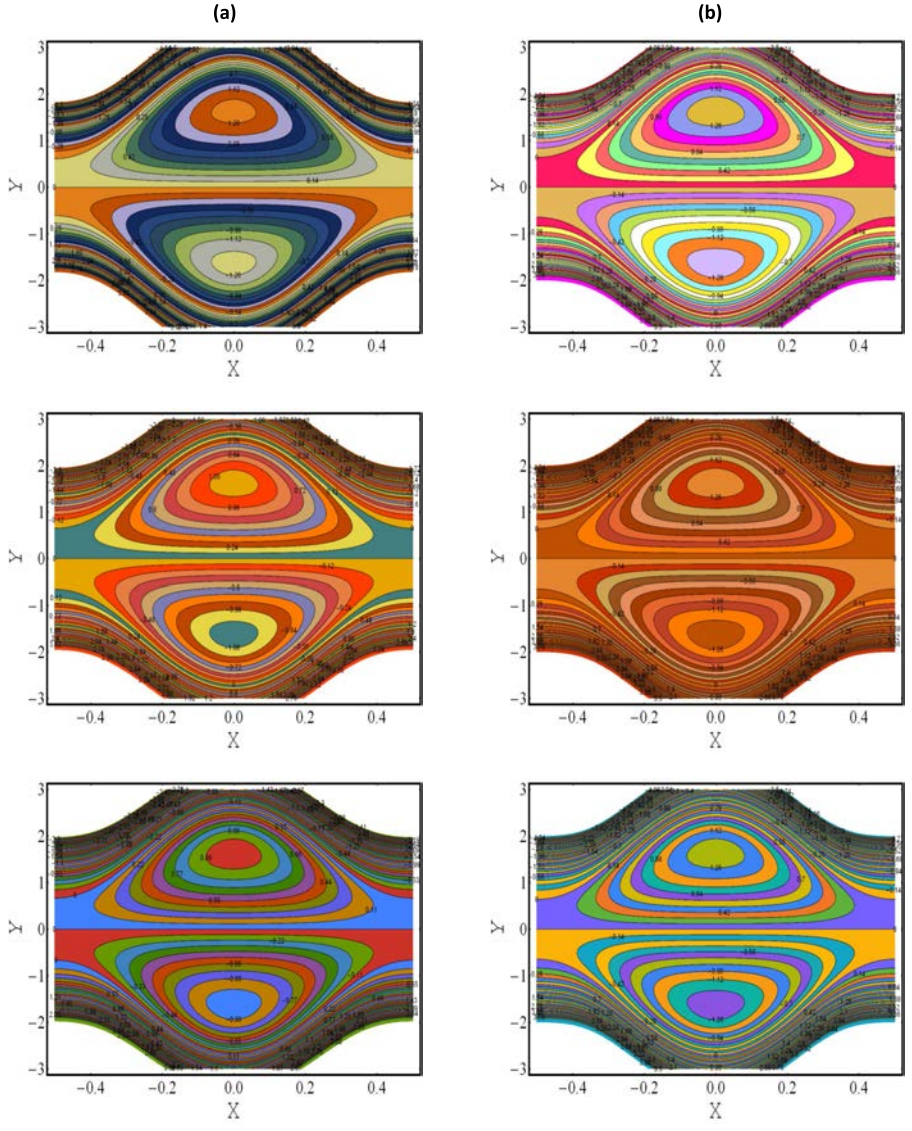

Fig. 16. (Color online) Streamlines for $P_v(0.1, 0.2, 0.3)$ when (a) $\lambda = 0.2$, $e = 0.5$, $\Lambda = 0$, $H = 1$, $\zeta = 1$. (b) $\lambda = 0.2$, $e = 0.5$, $\Lambda = 0.2$, $H = 1$, $\zeta = 1$.

constant. In Fig. 13(a), we observe that by increasing wavenumber λ the magnitude of bolus lessened passively also the size and number of bolus decreased. When the slip condition applies on it then magnitude is approximately constant also size and number of bolus remain the same as shown in Fig. 13(b). From Fig. 14(a), we predict that the Hartmann number has a very rapid effect on the magnitude of a bolus by increasing H. It is seen that by increasing values of Hartmann number, streamlines come to a close due to a decrease in flow strength, and the size of bolus decreases. This decrease is due to Lorentz forces which behave as retarding forces. From Fig. 15, we observe that by increasing the value of the Casson fluid parameter the magnitude of bolus decreases very gradually. Figure 16 depicted that by increasing the particle volume fraction (P_v) the magnitude of bolus decreased.

5. Conclusions

In this paper, the two-phase flow of Casson fluid is investigated. The main source of the flow is metachronal waves which are caused by the back and forth motion of cilia attached to the opposite walls of the channel. Hydro-magnetic flow experiences the effects of transverse magnetic fields incorporated with the slippery walls of the channel. A closed-form solution is obtained by solving differential equations with the assumption of long-wavelength and low Reynolds number. A comprehensive parametric study is carried out to infer the main contribution of the significant parameters. Some significant findings are enumerated below:

- The transport of Casson fluid is much slower than Newtonian fluid.
- A similar contribution of wavenumber (λ) and measure of the eccentricity parameter (e) is observed on the velocity of base fluid (u_f) under Casson fluid parameter ($\zeta \to \infty$) $\zeta \to 1$. But for slip conditions, the height of the graph is reduced when $\zeta = 1$.
- Hartmann number (H) and volume fraction (P_v) do not support the momentum of the fluid by reducing its velocity.
- More energy is added to the system for the Eckert number (e_k) and Prandtl number (P_r). While the heat of the system reduces for radiation parameters (r_d) in both types of multiphase flows.
- Under the thermal slip parameter, the height of the graph $\zeta \to 1$ is higher than the $\zeta \to \infty$ under no-slip conditions.
- The behavior of pressure rises for wavenumber λ is identical in all regions. In the comparison of non-Newtonian and Newtonian fluid graphs, firstly the height $\zeta \to 1$ is higher and then lower after the intersection for $\zeta \to \infty$.
- These results lead to the further analysis of metachronal wave and particle fluid.

Acknowledgment

The authors extend their appreciation to the Deanship of Scientific Research at King Khalid University, Abha 61413, Saudi Arabia for funding this work through research groups program under grant number R.G.P-1/234/42.

References

1. M. M. Bhatti, M. M. Rashidi and A. Zeeshan, *Eng. Sci. Technol. Int. J.* **20**, 265 (2016).
2. N. S. Akbar and Z. H. Khan, *J. Magn. Magn. Mater.* **378**, 320 (2015).
3. N. S. Akbar *et al.*, *Acta Astron.* **128**, 1 (2016).
4. Y. L. R. Quek, K. M. Lim and K. H. Chiam, *Comput. Fluids* **170**, 222 (2018).
5. M. Nazeer *et al.*, *Int. Commun. Heat Mass Transf.* **124**, 105274 (2021).
6. Y. Chu *et al.*, *Int. Commun. Heat Mass Transf.* **120**, 105011 (2021).
7. Y. Chu *et al.*, *Int. Commun. Heat Mass Transf.* **119**, 104980 (2020).
8. M. Nazeer *et al.*, *Numer. Methods Partial Differential Equations* 1 (2021).
9. M. Nazeer *et al.*, *J. Braz. Soc. Mech. Sci. Eng.* **41**, 518 (2019).
10. K. Ramesh *et al.*, *Phys. Scr.* **96**, 025225 (2021).
11. M. Nazeer *et al.*, *Eur. Phys. J. Plus* **134**(5), 204 (2019).
12. M. Nazeer, N. Ali and T. Javed, *J. Porous Media* **21**(10), 953 (2018).
13. M. Nazeer *et al.*, *Eur. Phys. J. Plus* **133**, 423 (2018).
14. M. Nazeer, N. Ali and T. Javed, *Canadian J. Phys.* **96**(6), 576 (2018).
15. M. Nazeer, N. Ali and T. Javed, *Canadian J. Phys.* **97**(1), 1 (2019).
16. M. W. Nazir *et al.*, *Numer. Methods Partial Differential Equations* 1 (2021), doi:10.1002/num.22768.
17. K. Ramesh, D. Tripathi and O. A. Bég, *Propul. Power Res.* **8**(3), 221 (2019).
18. F. Mebarek-Oudina *et al.*, *Int. J. Numer. Methods Heat Fluid Flow* **31**(4), 1172 (2020).
19. A. N. Ziam *et al.*, *J. Therm. Anal. Calorim.* **141**(5), 1981 (2020).
20. A. N. Ziam *et al.*, *Propul. Power Res.* **9**(4), 383 (2020).
21. F. Mebarek-Oudina, *Heat Transf.-Asian Res.* **48**, 135 (2019).
22. K. Ramesh *et al.*, *Phys. Scr.* **96**(2), 025225 (2020).
23. H. Firdous *et al.*, *Phys. Scr.* **96**, 025803 (2021).
24. F. Hussain *et al.*, *Z. Naturforsch.* (2021), https://doi.org/10.1515/zna-2021-0004.
25. M. Nazeer, SN *Appl. Sci.* **3**, 213 (2021).
26. M. Nazeer *et al.*, *Pramana – J. Phys.* **94**, 44 (2020).
27. Z. Fei *et al.*, *Appl. Therm. Eng.* **181**, 115881 (2020).
28. V. A. Rohachev *et al.*, *New J.* **20**, 100726 (2020).
29. J. Wang *et al.*, *Int. J. Heat Mass Transf.* **155**, 119719 (2020).
30. M. Nazeer *et al.*, *Surf. Interf.* **22**, 100803 (2021).
31. M. Nazeer *et al.*, *Surf. Interf.* **22**, 100846 (2021).
32. M. Nazeer *et al.*, *Phys. Scr.* **96**, 015201(2021).
33. M. Nazeer *et al.*, *J. Dispers. Sci. Technol.* doi:https://doi.org/10.1080/01932691.2021.1877557.
34. H. Ge-JiLe *et al.*, *Adv. Mech. Eng.***13**(3), 1 (2021).
35. A. Zeeshan *et al.*, *Int. J. Mod. Phys. B* **34**(11), 2050110 (2020).
36. N. Ali *et al.*, *Eur. Phys. J. Plus* **134**, 2 (2019).